OPTOELECTRONICS AND ADVANCED MATERIALS – RAPID COMMUNICATIONS Vol. 15, No. 11-12, November-December 2021, p. 538-545

Modelling of highly-sensitive graphene assisted silicon ring-resonator modulator for sensing applications

D. SHEKHAWAT*, R. MEHRA
Department of Electronics and Communication Engineering, Government Engineering College Ajmer, India

In the paper, the high performance silicon ring-resonator based intensity modulator is proposed which exhibits modulation based on the extent of the covering of the ring waveguide with graphene, and by electrical tuning of the chemical potential of the graphene. The deviation in the refractive index profile inside the graphene is responsible for modulation. The Q-factor of 900 throughout the entire C and L band gap is obtained. The high sensitivity and FSR of 0.83 nm/rad and 25 nm with switching rate of 10 dB/V is observed. The modulation efficiency of 100% is obtained at an angle of 4.5 rad.

(Received April 20, 2021; accepted November 24, 2021)

Keywords: Silicon, Ring-resonator, Nonlinear optics, Modulator

1. Introduction

Optical modulation [1] is a method of loading information onto the light beam. In general, this type of modulation is the result of changing the properties of the light beam such as direction, intensity, frequency, etc. Based on the physical characteristic of modulation, modulators are classified into electro-optical, all-optical, thermooptical [2-6]. Amongst them, all-optical, electro-optical, and thermo-optical modulators are the most general types of modulators because they are easily accessible with current materials and techniques. In electro-optical modulation, an electric field is used to control the beam parameters, including intensity as well as phase and thus shows fast modulation of the light [1]. Due to the ever increasing demand of optical communication the need of high speed modulators are obvious. Thus, in the recent past a large number of modulators have been reported [7-18]. Most of the optical modulators are demonstrated by Mach-Zehnder interferometer (MZI) [10-11] and, by ring resonator (RR) [12-18]. RR based modulators exhibits high modulation depth compared to MZI and other photonic structures Additionally, the dimensions of RR based devices are ultra-compact [17-18]. In the view of above advantages a new design of optical modulator using RR has been proposed in the paper.

The shifting of resonance wavelength in RR occurs by applying external potential which consequently, introduces optical intensity modulation in RR devices [13]. However, weak electro-optic coefficient of silicon needs large value of external potential to provide a phase shift of π. Thus, shift in the resonant peak of the RR is quite imperfect. RRs also possess various advantages like small bandwidth, large free spectral range (FSR) and high finesse. This in turn requires less tuning potential to switch the intensity from low to high output, hence enhancing the tuning efficiency of the modulator. The unwanted drifts in resonance due to the fabrication tolerance, temperature effects etc., limits the calibrations of the device. These limitations can be resolved by optimizing design and by the usage of graphene interactions [14]. Graphene with its extraordinary electrical properties has opened a wide area of silicon photonics based modulators [19]. Due to easy lab synthesis of graphene, many photonics components, for instance phase-shifters, photo-detectors, modulators, attenuators etc., have been demonstrated in silicon with embedded graphene [20].

In this paper, an optical modulator using silicon ring resonator (SRR) is proposed with the extent of the covering of the SRR with graphene layer. The graphene layer is employed to enhance the modulation efficiency. Graphene has extraordinary optical, electrical, and physicochemical properties, which shows its great potential in the designing of optical devices. The paper has investigated its optical properties using the FDTD method. The proposed modulator has a high sensitivity of resonant wavelength tuning with respect to both (i) external bias potential and (ii) graphene area. Moreover, these features have created fast modulation in the structure of the all-optical modulator.

In this paper, a compact and energy efficient modulator using graphene in silicon-on-insulator (SOI) waveguide of SRR is demonstrated. The introduction of disc shaped graphene in the proposed compact SRR modulator within the ring and coupling area increases the interaction region of the graphene with the ring and the

bus waveguide. Consequently, the efficiency of the modulator is also increases. The proposed device has been designed in single mode SOI waveguide to guide transverse electric mode. The proposed device is designed and simulated using "finite-difference-time–domain" (FDTD) based simulation platform to analyze the tunability of the wavelength characteristics of the SRR [21]. Finally, the tuning efficiency has been computed by varying device parameters, especially the graphene area or the disc angle and the external potential. The results obtained through the Lumerical's FDTD simulation are analyzed and validates our proposed scheme. The article is systematized as follows: in section 2, introduce and the working of SRR is described, in section 3, design and operation of the proposed device is explained, in section 4, results and discussions are highlighted and finally, in section 5, conclusion of the article is presented.

2. Working of graphene assisted SRR

Fig. 1(a) shows the model of the SRR structure whose radius is 5 μm. The cross-sectional view of the proposed device showing graphene and metal layers are labelled in Fig. 1(b). The proposed device consists of the bus waveguide, the ring waveguide, the top layer graphene as well as the Al_2O_3 contact deposited on SiO_2 layer. The schematic simulation set-up designed in FDTD simulation platform is shown in Fig. 1 (c). The electric field evolution in the proposed device is shown in Fig. 1(d).

The simulation parameters are selected and optimized through FDTD simulation software. The geometrical parameters are optimized in such a way that the optimum performance of the device can be obtained [21]. In simulation, first of all we have chosen rectangular waveguide because it confines light in both x and y dimensions and for compatibility on SOI (silicon-on-insulator) technology, as well. Then the width and height of the waveguide is optimized and selected as 0.55 μm and 0.25 μm in such a way that it supports fundamental mode of light as well as it is suited for SOI platform. We have used high-index-contrast waveguides of Si-SiO_2 material combination to support our small bending radius of MRR.

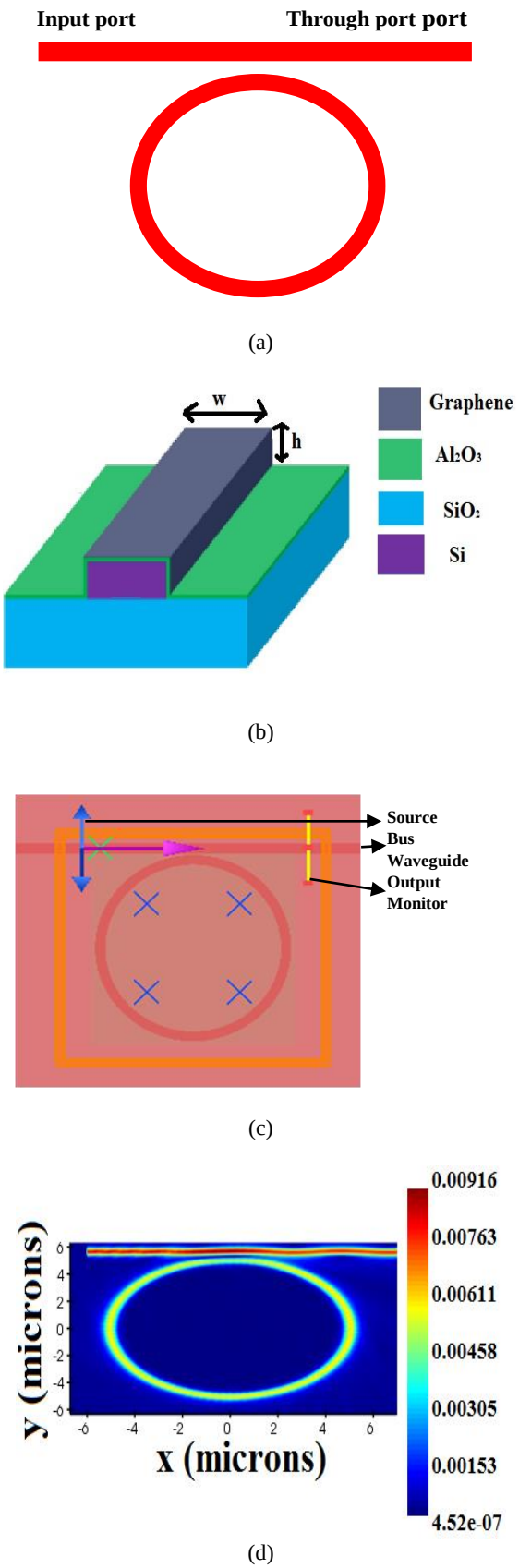

Fig. 1. (a) Schematic of a SRR (b) Cross-sectional of the waveguide of the proposed RR (c) Simulation set-up of the proposed device in the FDTD platform (d) Electric field evolution in the proposed device (color online)

The radius, coupling length, the gap between straight and ring waveguide as well as height-width of the waveguide is optimized through FDTD simulation. As seen from optimization, if the radius is 3 µm, there is less losses due to modal mismatch. Then we optimized coupling length and gap between straight and bend waveguide by trial and error method in FDTD simulation. At coupling length 1.5 µm with gap 0.1 µm, we found that maximum 90% of input light coupled to the ring. While for radius, coupling length and gap of 5 µm, 2 µm, and 0.1 µm, 85% of light coupled to the ring respectively. We have chosen rectangular waveguide because it confines light in both x and y dimensions and for compatibility on SOI (silicon-on-insulator) technology. We have selected width and height of waveguide as 0.55 µm and 0.25 µm in such a way that it supports fundamental mode of light as well as it is suited for SOI platform. We have used high-index-contrast waveguides of Si-SiO_2 material combination to support our small bending radius of MRR. The key parameters are stated in Table 1. The selected material combination is Si/SiO_2 which possesses tightly confined guided modes and compatible with e-beam lithography technique. The transfer function of the modulator is written below [15].

$$E_t = \frac{D\sqrt{1-k_1} - D\sqrt{1-k_2}x^2\exp^2(j\phi)}{1-\sqrt{1-k_1}\sqrt{1-k_2}x^2\exp^2(j\phi)} E_{i1} + \frac{-D\sqrt{k_1}\sqrt{k_2}x\exp(j\phi)}{1-\sqrt{1-k_1}\sqrt{1-k_2}x^2\exp^2(j\phi)} E_{i2} \quad (1)$$

where $\phi = \frac{k_n L}{2}$, $x = D.\exp\left(-\alpha\frac{L}{4}\right)$, $D = (1-\gamma)^{\frac{1}{2}}$ and L is the circumference of the ring which is equal to 2πR and κ is the coupling coefficient between waveguides of SMRR. The E_{i1} is the input electric field applied through the input port and E_{i2} = 0 as no input is applied through the add port of the RR. The other variables of Eq (1) are explained in [15]. The change in refractive index (Δn) and excess loss (Δα) at 1.55 µm, inside the SRR after applying the external voltage has been be expressed below [16].

$$\Delta n = \Delta n_e + \Delta n_h$$
$$\Delta n = -[\,8.8\times10^{-22}\Delta N_e + 8.5\times10^{-18}(\Delta N_h)^{0.8}] \quad (2)$$

$$\Delta\alpha = \Delta\alpha_e + \Delta\alpha_h$$
$$\Delta\alpha = [\,8.5\times10^{-18}\Delta N_e + 6.0\times10^{-18}\Delta N_h] \quad (3)$$

$\Delta N_e, \Delta N_h$ are the concentration of free electron and free holes expressed in cm^{-3}. The magnitude response of a typical SRR having κ value equal to 0.03 is considered in the paper, at different gate voltages. Eq (1) is used to study and determine the transmission nature of the proposed device as well as it has been used to compare with output transmission graph of the model as obtained from simulation.

Table 1. Parameters used in designing the model

S. No.	Parameters	Value
1.	Height of the waveguide (h)	250 nm
2.	Width of the waveguide (w)	550 nm
3.	Height of the slab	150 nm
4.	Graphene	C (graphene)-(mid-IR)
5.	Thickness of the graphene layer	0.1 nm
6.	Thickness of the Al_2O_3 contact	7 nm
7.	Simulation platform used	FDTD
8.	Radius of the RR	5 µm
9.	Refractive Index of SiO_2	1.55
10.	Refractive Index of Si	3.20
11.	Refractive Index of Al_2O_3	1.6

Moreover, the gate voltage is also responsible for the change in the chemical potential of the top graphene sheet. The variation of the chemical voltage with the gate voltage is shown in Fig. 2. The bias voltage causes perturbation in the RI as well as in the loss coefficient of the SRR and thus, operates as an intensity modulator as described in [12, 22].

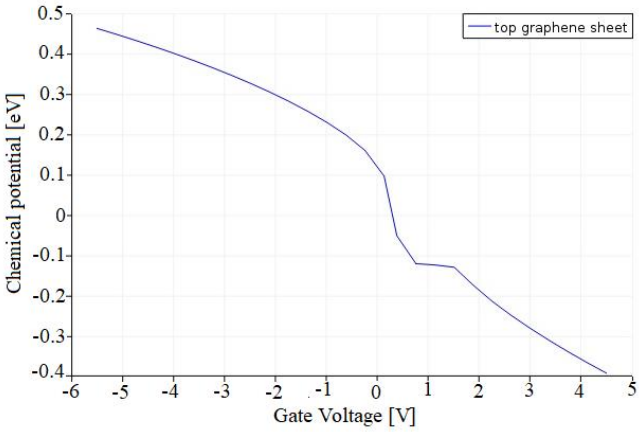

Fig. 2. Variation of the chemical potential of the top graphene sheet

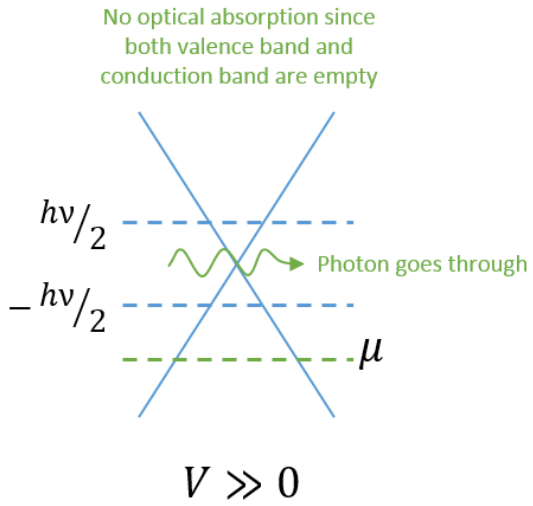

(a)

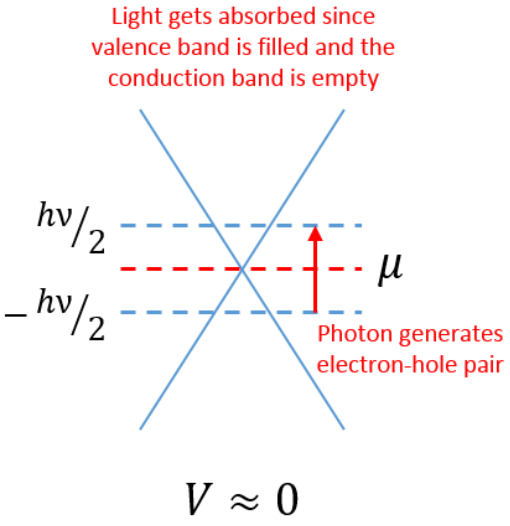

(b)

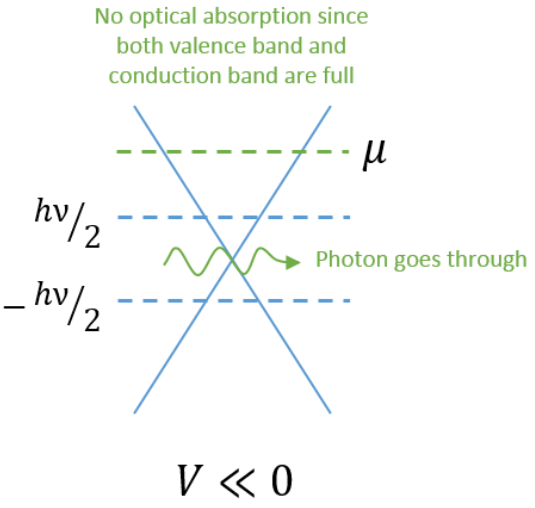

(c)

Fig. 3. Modulation in graphene's optical absorption with different applied bias voltage (color online)

In the proposed device, the external gate potential is applied at the electrode to change the chemical potential of the graphene. Consequently, a change in chemical potential changes the effective RI of the waveguide. Thus, there is a variation in the resonance wavelength of the SRR modulator and can be shifted by tuning the external biased voltage [19, 23]. The proposed device achieves modulation by tuning the "Fermi level" of the graphene layers. The applied voltage in the graphene shifts its Fermi level modifies its "optical absorption rate" and consequently, modulates the optical response of the silicon waveguide. An illustration of the modulation with applied bias voltage in graphene is shown in Fig. 3.

The carrier density of the graphene can be changed by altering the voltage on the metal electrode of the gate of the device, which can be expressed as [15, 19].

$$n_s = \frac{2}{\pi\hbar^2 V_F^2}\int_0^\infty \varepsilon[f_d(\varepsilon) - f_d(\varepsilon + 2\mu_c)]d\varepsilon \qquad (4)$$

where $f_d(\varepsilon)$ is the Fermi-Dirac distribution function, μ_c is the chemical potential and V_F is the applied voltage. The voltage used to tune the graphene can be expressed below [16, 23].

$$\mu_c = \hbar v_F \sqrt{\pi\eta|(V_0 - V_D)|} \qquad (5)$$

The effect of external voltage has been used to compute chemical potential of graphene using analytic Eq. (5). Eq. (5) utilized to analyze the system as well as to verify the simulated results. Further the chemical potential gives us effective index of graphene and the same effective index has been used for graphene responding to the voltage that we have used.

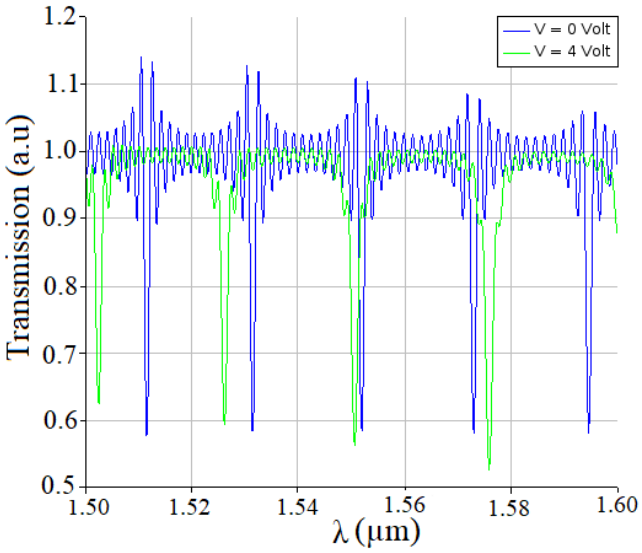

Fig. 4. Transmission spectrum at the output of the proposed device (color online)

In Fig. 4 the resonance-shift possess fluctuations when V = 0 which is due to high refractive index contrast of the device. While when V = 4V, the fluctuations occurred due to the change in the chemical potential of the graphene. The chemical potential of graphene is changed in such a way that the effective refractive index contrast is reduced during propagation and thereby causing the fluctuations in the resonance-shift of the spectrum.

Fig. 4 depicts the output response of the device, if the external applied voltage is altered from 0 V to 4 V respectively. The rate of wavelength tuning with respect to the external bias gate voltage is obtained as high as 1.25 nm/V as observed from the simulated output graph as depicted in Fig. 4. Voltage has been applied to observe steady state response to switch the output intensity from 0 V to 1 V and vice-versa. While the speed of the proposed device is obtained from the transient and the small signal model analysis, which is found to be 25 Gbps. Despite low speed of operation compared to optical pumping devices, the proposed device is more compact in size (as radius is 3μm) respectively [23-24].

Similarly, the optical modulation as well as wavelength shift is observed by varying the covering area of the ring of the SRR. The graphene available in the material database of the FDTD simulation is selected for simulation and considered the following mathematical form for computation [17, 21].

$$\varepsilon_{XX} = \varepsilon_{YY} = x_6 - \frac{x_1^2 x_3}{\pi x_2^2} \frac{\omega}{\omega^2 + \left(\frac{x_1 x_4^2}{x_5 x_3}\right)^2} \frac{1}{\omega x_8 x_7} + i \frac{x_1^2 x_3}{\pi x_2^2} \frac{\omega}{\omega^2 + \left(\frac{x_1 x_4^2}{x_5 x_3}\right)^2} \frac{x_1 x_4^2}{\omega x_5 x_3 x_8 x_7} \quad (6)$$

where

v_f : *Fermi velocity*, μ : *carrier mobility*, $x_1 = e$ (C), $x_2 = \hbar$ (J-s), $x_3 = \mu_c$(J), $x_4 = v_f$ (m/s), $x_5 = \mu$ (Carrier mobility m^2/V/s), $x_6 = \varepsilon_r$, $x_7 = \Delta$ (m), $x_8 = \varepsilon_0$(F/m).

3. Modeling of graphene assisted SRR

In this work, a single SRR is modulated in with the variation of the graphene covering from the top of the ring waveguide. Fig. 5 displays the SRR modulator without graphene and with half and full graphene covering of the ring waveguide of the SRR modulator. The corresponding output spectrum of the graphene assisted SRR is depicted in Fig. 6.

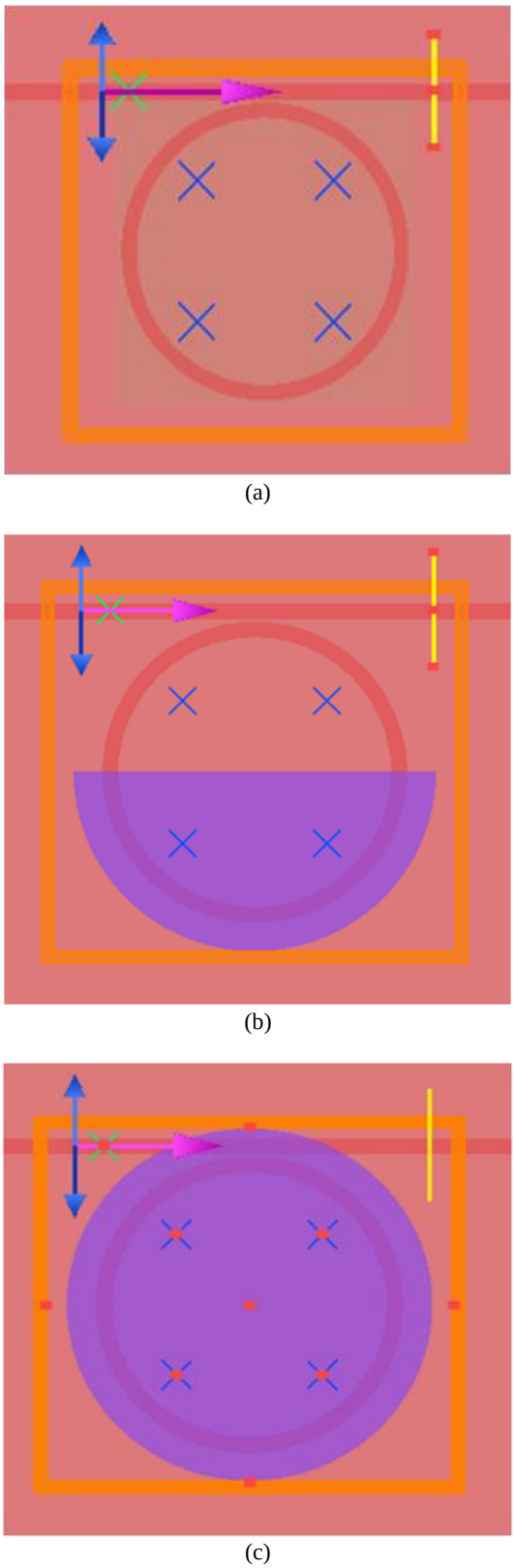

(a)

(b)

(c)

Fig. 5. Schematic of FDTD simulation environment of Graphene assisted Ring Resonator (a) without Graphene, (b) with Half Disk Graphene, and (c) Full Disk Graphene (color online)

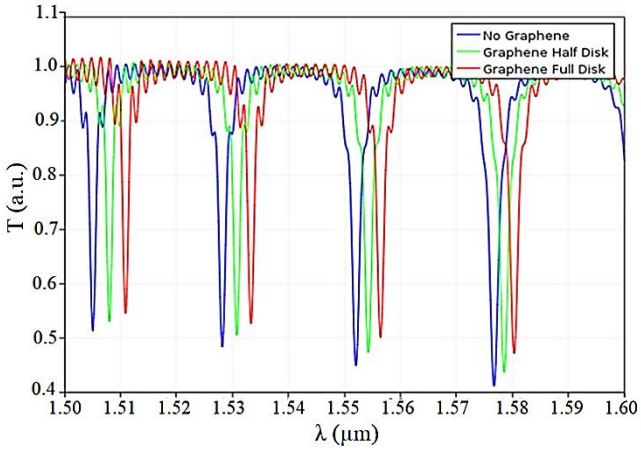

Fig. 6. Transmission spectrum generated after the FDTD Simulation of Graphene assisted Ring Resonator (a) without Graphene (blue colour), (b) with Half Disk Graphene (green colour), and (c) Full Disk Graphene (red colour) (color online)

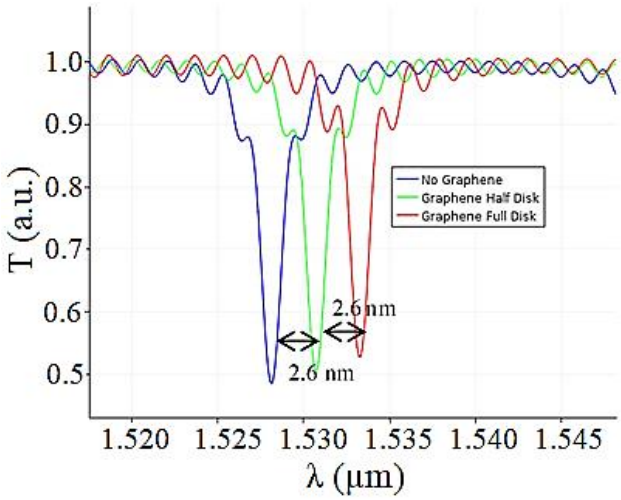

Fig. 7 Magnified view of Transmission spectrum generated after the FDTD Simulation of Graphene assisted Ring Resonator showing relative resonant shifts and intensity modulations (a) without Graphene (blue colour), (b) with Half Disk Graphene (green colour), and (c) Full Disk Graphene (red colour) (color online)

The usage of graphene responsible for a net change in the RI and thus a resonant wavelength shift occurs inside SRR. Fig. 6 shows the transmission spectrum generated after the FDTD simulation of graphene assisted SRR, without graphene, with half-disc graphene and full disc graphene. The magnified view of the same is shown in Fig. 7. We have used the angle of disc as π and to 2 π because the shape of disc becomes symmetrical to the coupling region. It can be observed that as the amount of covering of the graphene increases, the red-shift occurs. If the ring is fully covered with graphene, the transmission graph is shifted to 5.2 nm. Also, the shift can be approximated linear with respect to the graphene covering angle. However, non-linearity may occur if the placement of graphene is asymmetric with respect to coupling region. The disc with angle $\pi/2$ and $3\pi/2$ will be asymmetrical in the coupling region which in turn will introduce wavelength dependent transmission spectrum which is not required. That is why, the graphene angle of interest selected for simulation are symmetric with respect to the coupling region. Using graphene disc we are not claiming any absolute sensitivity. However, the sensitivity increases relatively as we have calculated the rate of wavelength shift with respect to external voltage applied when graphene is present and this relative sensitivity is pretty much good. Further it can be used for switching and sensing purposes. Thus, it can be concluded that this novel technique may be applied to obtain the intensity modulation in the SRR. Further, the same SRR model may hence be used as on-off switching and/or RI sensing purpose.

4. Simulation results and discussion

The proposed device is designed and modelled in Lumerical FDTD environment [17, 21]. Material properties and simulation parameters used for simulation are listed in Table 1. The resonance shift with respect to angle subtended by graphene disc at the centre of the ring is illustrated in Fig. 7. Similarly, resonant wavelength shift of ~ 2.6 nm is recorded when graphene start and end angle was changed from 0-360 degree to 180-0 degree. Fig. 8 shows the shifting of resonance when graphene angle is varied. Eq. 3 and Eq. 4 shows the variation in RI as well as in the loss profile which has been determined by eigenmode solver and propagator [17, 21]. The variation of wavelength-shift with the change in disc angle is listed in Table 2. Fig 9 shows the transmission spectrum showing intensity modulation and modulation sensitivity generated after the FDTD simulation of the proposed SRR. The relative resonant shifts and intensity modulations are shown the figure below.

Table 2. Variation of Disc angle and respective wavelength shift

Disc angle θ [rad]	λ [nm]	Δλ [nm]
0	1528	0
π	1530.6	2.6
2 π	1533.2	5.2

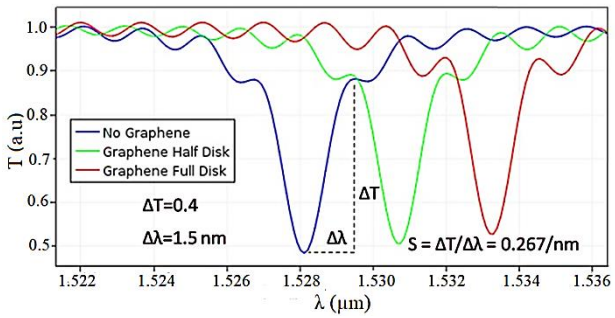

Fig. 8. Transmission spectrum showing intensity modulation and modulation sensitivity generated after the FDTD simulation of graphene assisted SRR showing relative resonant shifts and intensity modulations (a) without graphene (blue colour), (b) with half disc graphene (green colour), and (c) full disc graphene (red colour) (color online)

In order to investigate the performance of the proposed scheme, the various characteristic parameters are defined and calculated below [25-29].

Free Spectral Range (FSR) - FSR (Δλ) estimated by calculating the difference between consecutive resonances wavelength in the transmission spectrum of MRR. Here FSR of 25 nm is obtained when graphene is placed to cover the device, as shown in Fig. 6.

Full-width at half maximum (FWHM) - is the width of transmission spectrum curve at 3dB attenuation level for respective resonance. Here FWHM of 4 nm is observed.

Finesses (F) - Finesses is defined by the ratio of FSR and FWHM of the ring resonator which is found to be 6.25.

Quality-factor (Q) – is the energy stored inside the SRR divided by the energy lost per circulation of the field in the SRR [20, 21]. Here the Q has been found to be 900.

$$\mathrm{Q} = \frac{\text{Stored energy}}{\text{Power lost}} \tag{7}$$

Sensitivity - The resonant wavelength sensitivity with respect to the angle subtended by graphene disc at the centre of the ring can be defined below.

$$S_\theta^\lambda = \frac{\Delta\lambda}{\Delta\theta}\ (nm/rad) \tag{8}$$

It can be computed from Table 2 as $S_\theta^\lambda = \frac{2.6}{\pi} = 0.83\frac{nm}{rad}$. The transmission intensity sensitivity with respect to the shift in resonant wavelength can be defined below.

$$S_\lambda^T = \frac{\Delta T}{\Delta\lambda}(/\mathrm{nm}) \tag{9}$$

And the same can be computed from Fig. 8 as $S_\lambda^T = 0.267\ /nm$ (since $\Delta T = 0.4$, and $\Delta\lambda = 1.5\ nm$ from Fig. 8).

Therefore, the resultant (or overall) intensity modulation sensitivity with respect to angle subtended by graphene disc at the centre of the ring is defined below.

$$S_\theta^T = \frac{\Delta T}{\Delta\theta} = \frac{\Delta T}{\Delta\lambda} \times \frac{\Delta\lambda}{\Delta\theta}(/\mathrm{rad}) \tag{10}$$

It can be computed as $S_\theta^T = \frac{\Delta T}{\Delta\theta} = 0.267 \times 0.83\ /\ rad$, or $S_\theta^T = 0.222\ (/rad)$. From Eq. (10), the following important results can be deduced.

1. Full disc intensity modulation = $2\pi \times 0.222 = 1.33$ which is more than 100%
2. Angle required for 100% intensity modulation = 1/(0.222/rad) = 4.5 rad.

The sensitivity of the device with respect to graphene length is noted as high as around 6 nm/μm with a switching rate of 10 dB/V which is measured directly from the transmission spectrums at 0 V and at 1 V by measuring the slope in dB per nm and multiplying it by shift in nm per unit volt. However the switching time of the proposed model is 0.2 ps.

Thus, from the above results, it can be concluded that the graphene assisted SRR modulator has higher sensitivity compared to other without graphene assisted SRR modulator. The device footprint is calculated and found to be 130 μm^2 [23, 24]. The reason for low ER in the device is due to the small ring architecture. Therefore, the observable figure of merit for the proposed scheme is (i) compact size, (ii) small graphene area which provides easiness to fabricate to the device, (iii) less driving power for on-off switching of the modulator.

5. Conclusion

The proposed architecture using graphene based SRR modulator is designed and simulated at different gate potentials. The device is modelled using FDTD based numerical simulation platform. The modulation is obtained if gate potential changed or the disc covering area is altered. The wavelength shift in resonance wavelength is observed by varying small chemical potential of graphene. The high tuning rate of around 1.25nm/V is achieved by covering ring geometry of the device using graphene. The proposed architecture is compact with the size of 130 μm^2 and suitable for both SOI platform and for CMOS. The sensitivity of the device is noted as high as around 0.83 nm/rad with the switching rate of 10 dB/V. The device may also play an outstanding role for future modulation technique. Therefore, the proposed concept proved to be a dominating candidate for the future optical modulators, packet switches as well as all-optical information processing schemes in data-centers where the optical modulation techniques are required.

References

[1] G. T. Reed, G. Mashanovich, F. Y. Gardes, D. J. Thomson, Nature Photonics **4**, 518 (2010).

[2] R. Vilson Almeida, Carlos A. Barrios, Roberto R. Panepucci, Michal Lipson, Nature **431**, 1081 (2004).

[3] Qianfan Xu, Bradley Schmidt, Sameer Pradhan, Michal Lipson, Nature **435**, 325 (2005).

[4] G. Cocorullo, I. Rendina, Electronics Letters **28**(1), 83 (1992).

[5] David Petrosyan, Yuri P. Malakyan, Physical Review A **70**, 023822 (2004).

[6] Berg, "Acousto-optic signal processing: theory and implementation", CRC Press, 1995.

[7] G. T. Reed, F. Y. Gardes, D. J. Thomson, Hu Y, J. Fedeli, G. Mashanovich, Frontiers in Physics **2**, 77 (2014).

[8] G. T. Reed, G. Mashanovich, F. Y. Gardes, M. Nedeljkovic, Y. Hu, D. J. Thomson, K. Li, P. R. Wilson, S. Chen, S. Hsu, Nanophotonics **3**(4), 229 (2013).

[9] G. Zhou, M. W. Geis, S. J. Spector, F. Gan, M. E. Grein, R. T. Schulein, J. S. Orcutt, J. U. Yoon, D. M. Lennon, T. M. Lyszczara, E. P. Ippen, F. Käertner, Optics Express **16**(8), 5218 (2008).

[10] A. Liu, R. Jones, L. Liao, D. Samara-Rubio, D. Rubin, O. Cohen, R. Nicolaescu, M. Paniccia Nature **427**, 615 (2004).

[11] H. Xu, X. Li, X. Xiao, Z. Li, Y. Yu, J. Yu, IEEE Journal of Selected Topics in Quantum Electronics **20**(4), 23 (2013).

[12] S. Pal, S. Gupta, IEEE Transactions on Nanotechnology **18**, 392 (2019).

[13] G. Li, A. V Krishnamoorthy, I. Shubin, J. Yao, IEEE Journal of Selected Topics Quantum Electronics **19**(6), 95 (2013).

[14] F. Zhou, H. Wen, X. Jin, Asia Communications and Photonics Conference OSA Technical Digest (online) paper Su2A.151 (2017).

[15] J. K. Rakshit, T. Chattopadhyay, J. N. Roy, Theoretical and Applied Physics **1**, 32 (2013).

[16] B. B. Bhowmik, S. Gupta S, Optics Communications **349**, 132 (2015).

[17] G. K. Bharti, J. K. Rakshit, Optical Engineering **60**(3), 035103 (2021).

[18] G. K. Bharti, J. K. Rakshit, M. P. Singh, P. Yupapin Journal of Nanophotonics **13**(3), 036002 (2019).

[19] M. Danaeifar, N. Granpayeh, A. Mohammadi, A. Setayesh, Applied Optics **52**(22), 68 (2013).

[20] M. Liu, X. Yin, E. Ulin-Avila, B. Geng, T. Zentgraf, L. Ju, F. Wang, X. Zhang, Nature **474**, 64 (2011).

[21] [Online] https://www.lumerical.com/products.

[22] Y. Ding, X. Zhu, S. Xiao, H. Hu, L. H. Frandsen, N. A. Mortensen, K, Yvind, Nano Letters **15**(7), 4393 (2015).

[23] J. K. Rakshit, K. E. Zoiros, G. K. Bharti, Journal of Computational Electronics **20**(1), 353 (2021).

[24] J. K. Rakshit, J. N. Roy, Optica Applicata **46**(4), 517 (2016).

[25] M. P. Singh, J. K. Rakshit, U. Biswas, G. K. Bharti, A. Tiwari A (2020), International Conference on Computational Performance Evaluation (ComPE), Shillong, India 978-1-7281-6644-5, (2020).

[26] G. K. Bharti, M. P. Singh, J. K. Rakshit, Silicon **12**, 1279 (2019).

[27] P. Sah, B. K. Das, Applied Optics **57**(9), 2277 (0218).

[28] G. K. Bharti, J. K. Rakshit, Optoelectron. Adv. Mat. **13**(1-2), 10 (2019).

[29] G. K. Bharti, U. Biswas, J. K. Rakshit, Optoelectron. Adv. Mat. **13**(7-8), 407 (2019).

*Corresponding author: deepakphdgeca@gmail.com